

The Persistent Eruption of UGC 2773-OT: Finally, a Decade-Long Extragalactic Eta Carinae Analog

Nathan Smith^{1*}, Jennifer E. Andrews¹, Jon C. Mauerhan², WeiKang Zheng², Alexei V. Filippenko², Melissa L. Graham², and Peter Milne¹

¹*Steward Observatory, University of Arizona, 933 N. Cherry Ave., Tucson, AZ 85721, USA*

²*Department of Astronomy, University of California, Berkeley, CA 94720-3411, USA*

26 August 2018

ABSTRACT

While supernova (SN) impostors resemble the Great Eruption of η Carinae in the sense that their spectra show narrow H lines and they have typical peak absolute magnitudes of -13 to -14 mag, most extragalactic events observed so far are quite different from η Car in duration. Their bright phases typically last for ~ 100 d or less, rather than persisting for several years. The transient object UGC 2773-OT (discovered in 2009) had a similar peak absolute magnitude to other SN impostors, but with a gradual 5-yr predisccovery rise. In the ~ 6 yr since discovery, it has faded very slowly (0.26 mag yr⁻¹). Overall, we suggest that its decade-long eruption is so far the best known analog of η Car’s 19th century eruption. We discuss extensive spectroscopy of the ongoing eruption. The spectra show interesting changes in velocity and line shape that we discuss in detail, including an asymmetric H α emission line that we show is consistent with the ejection of a bipolar nebula that could be very much like the Homunculus of η Car. Moreover, changes in the line width, line profile, blue excess emission resembling that of Type II_n supernovae, and the intensity of H α suggest the presence of strong circumstellar interaction in the eruption at late times. This supports the hypothesis that the extended plateau of η Car’s eruption may have been powered by shock interaction as well. One interesting difference compared to η Car, however, is that UGC 2773-OT so far does not exhibit the repeated brief spikes in luminosity that have been associated with binary periastron events.

Key words: circumstellar matter — stars: evolution — stars: winds, outflows

1 INTRODUCTION

Observations indicate that there is a population of eruptive or explosive visible-wavelength transient sources that are systematically less luminous than supernovae (SNe), but more luminous than any stable star. Historically (Humphreys, Davidson, & Smith 1999), four examples were known: P Cygni in 1600 AD, η Carinae’s 19th century eruption (both in the Milky Way), SN 1954J in NGC 2403 (also known as Variable 12), and SN 1961V in NGC 1058. These were considered to be giant eruptions of luminous blue variable stars (LBVs). SN 1961V has since (Smith et al. 2011; Kochanek et al. 2011) turned out to be a likely core-collapse SN of Type II_n (SN II_n), but among the others, η Carinae’s eruption is often regarded as the proto-

type of these giant LBV eruptions, albeit the most extreme example.

Modern surveys for SNe have serendipitously found a few dozen of these luminous eruptive stars that were sometimes (especially in earlier studies) considered to be analogs of η Carinae and the LBVs. Because they are typically found in systematic surveys intended to find SNe, they are often called “SN impostors” (Van Dyk & Matheson 2012), although they have also been referred to as η Car analogs, Type V SNe, intermediate-luminosity transients, and other names (Goodrich et al. 1989; Van Dyk et al. 2000; Van Dyk 2005; Zwicky 1961, 1965). See Smith et al. (2011) and Van Dyk & Matheson (2012) for recent general reviews of these eruptive sources, as well as many references therein regarding individual objects. Kochanek (2011) has discussed considerations of the important role of dust in these events.

As more examples of these SN impostors have been dis-

* E-mail: nathans@as.arizona.edu

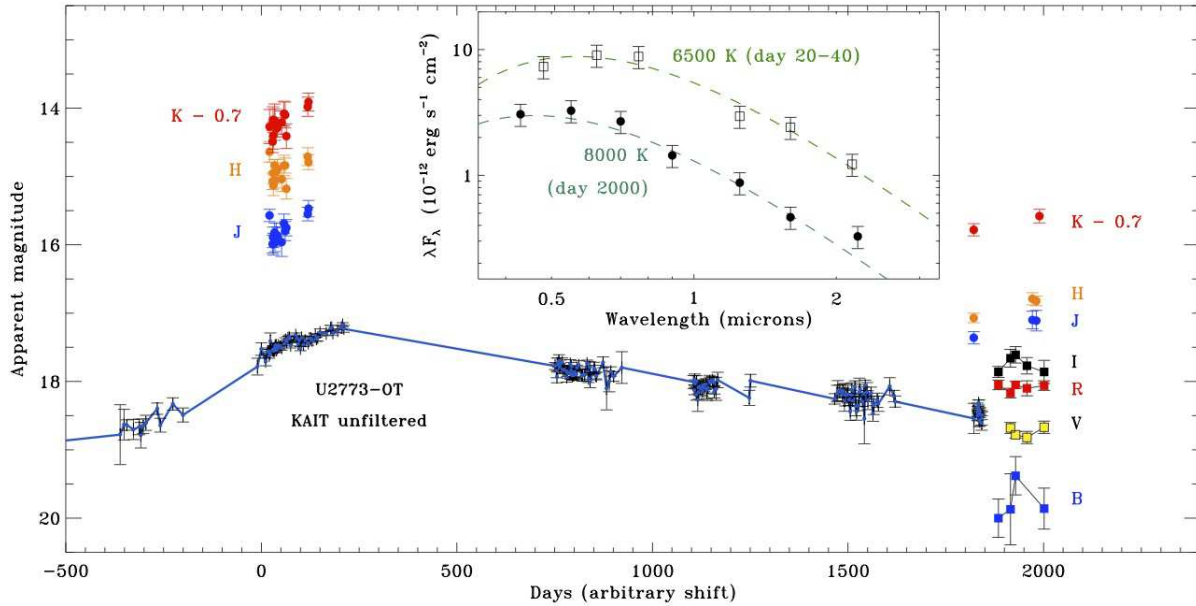


Figure 1. The observed apparent magnitude light curve of UGC 2773-OT in multiple bands, including the KAIT unfiltered light curve (calibrated as *R*), the early *JHK* points from Smith et al. (2010), late-time *BVRi* from the Kuiper telescope, and *JHK* measurements from UKIRT (see Tables 1 and 2). The inset shows the dereddened SED at early times and late times.

covered, and as more examples have been studied in detail, it has become increasingly clear that there is a wide diversity among SN impostors, and that few of them are actually close analogs of η Car’s historical eruption. Some classic SN impostors have luminous, hot, blue progenitors and an indication that the star survived the eruption, such as SN 1997bs (Van Dyk et al. 2000) and SN 2009ip¹ (Smith et al. 2010; Foley et al. 2011). A somewhat different subset of SN impostors includes SN 2008S, the 2008 optical transient in NGC 300, SN 2010dn, and similar objects that are sometimes referred to as intermediate-luminosity red transients because of the cooler photospheres that develop (Berger et al. 2009; Bond et al. 2009; Kochanek et al. 2011, 2012; Thompson et al. 2009; Prieto et al. 2008a; Smith et al. 2009a, 2011; Wesson et al. 2010). Most of these exhibit characteristic bright emission in the infrared (IR) lines of Ca II and [Ca II], perhaps related to their dusty circumstellar matter (CSM) (Prieto et al. 2008a; Smith et al. 2011). The most interesting property of these is that there are a few cases where a deeply dust-enshrouded and relatively low-luminosity progenitor (perhaps a super-asymptotic giant branch [AGB] star) has been identified in pre-eruption IR data (Prieto 2008; Prieto et al. 2008a; Thompson et al. 2009). Some objects share properties of both categories, like UGC 2773-OT (the object discussed in this paper), which had a luminous blue progenitor and developed the [Ca II] and Ca II emission that is characteristic of the SN 2008S-like transients (Smith et al. 2010, 2011; Foley et al. 2011). SN 2002bu shows properties of both classes as well, changing as it faded (Smith et al. 2011; Szczygiel et al. 2012). SN Hunt248 was an LBV-like erup-

tion that appeared to arise from a yellow hypergiant progenitor (Mauerhan et al. 2015), and SN 2003gm may have been as well (Maund et al. 2006).

Additionally, a subset of the SN impostors show very brief (lasting a few weeks) flares in optical luminosity that fade quickly and in many cases repeat, and sometimes precede a larger outburst. Some examples of these flares are seen in SN 2000ch, SN 1954J before its 1954 peak, and the pre-SN eruptions of SN 2009ip (Humphreys, Davidson, & Smith 1999; Smith et al. 2010; Pastorello et al. 2010; Smith et al. 2011; Mauerhan et al. 2013; Wagner et al. 2004). Similar brief peaks were seen in η Car’s Great Eruption too², and are hypothesised to be related to stellar collisions at periastron in an eccentric binary system (Smith 2011). Finally, some SN impostors and giant LBV eruptions have substantially less luminous peaks than η Car, with peak luminosities of -10 to -11 mag, rather than -14 mag. Examples of these fainter eruptions are P Cygni’s 17th century eruptions, SN 1954J, SN 1954kg (although we caution that SN 2002kg may have actually been a normal S Dor eruption and not a giant eruption; Maund et al. 2006; Van Dyk et al. 2006), V1 in NGC 2366 (Drissen et al. 2001) and the 1990s eruption of HD 5980 in the Small Magellanic Cloud (see Koenigsberger et al. 2004). Thus, there is a very wide diversity among this class of eruptions, if indeed they belong in the same class.

Kochanek et al. (2012) have pointed out that most SN impostors do not match traditional expectations for LBV giant eruptions as summarised by Humphreys & Davidson (1994), and suggest that many of them are more likely to be SN 2008S-like events. This may partly be an expres-

¹ SN 2009ip later appeared to explode as a SN in 2012 (Mauerhan et al. 2013), but the star survived its pre-2012 eruptions.

² These “flashes and relapses” are what led John Herschel to describe η Car as “fitfully variable to an astonishing extent” Herschel (1847).

Table 1. Unfiltered KAIT Photometry of UGC 2773-OT

| MJD | mag | 1σ (mag) |
|---------|-------|-----------------|
| 55051.5 | 17.78 | 0.12 |
| 55061.5 | 17.52 | 0.09 |
| 55812.5 | 17.77 | 0.05 |
| 55816.5 | 17.84 | 0.10 |
| 55817.4 | 17.93 | 0.09 |
| 55818.4 | 17.76 | 0.10 |
| 55820.4 | 17.72 | 0.06 |
| 55822.5 | 17.70 | 0.09 |
| 55824.5 | 17.79 | 0.05 |
| 55826.5 | 17.74 | 0.06 |
| 55830.5 | 17.72 | 0.06 |
| 55832.5 | 17.83 | 0.06 |
| 55836.5 | 17.83 | 0.05 |
| 55842.4 | 17.94 | 0.07 |
| 55843.4 | 17.85 | 0.07 |
| 55844.4 | 17.88 | 0.07 |
| 55851.5 | 17.74 | 0.06 |
| 55852.5 | 17.89 | 0.08 |
| 55853.5 | 17.84 | 0.06 |
| 55854.4 | 17.78 | 0.06 |
| 55855.5 | 17.90 | 0.06 |
| 55856.5 | 17.91 | 0.06 |
| 55857.5 | 17.90 | 0.08 |
| 55858.5 | 17.89 | 0.06 |
| 55859.5 | 17.89 | 0.06 |
| 55860.5 | 17.91 | 0.06 |
| 55862.4 | 17.86 | 0.07 |
| 55864.5 | 17.88 | 0.06 |
| 55866.5 | 17.90 | 0.06 |
| 55868.4 | 17.80 | 0.03 |
| 55873.3 | 17.76 | 0.06 |
| 55880.4 | 17.92 | 0.05 |
| 55882.4 | 17.91 | 0.08 |
| 55882.4 | 17.91 | 0.08 |
| 55888.4 | 17.90 | 0.09 |
| 55894.4 | 17.73 | 0.05 |
| 55898.3 | 17.96 | 0.06 |
| 55901.3 | 17.79 | 0.08 |
| 55902.2 | 17.99 | 0.10 |
| 55912.3 | 17.81 | 0.09 |
| 55914.3 | 17.83 | 0.06 |
| 55916.2 | 17.91 | 0.05 |
| 55918.3 | 17.92 | 0.05 |
| 55935.2 | 17.72 | 0.08 |
| 55944.2 | 18.10 | 0.31 |
| 55951.1 | 18.00 | 0.15 |
| 55955.1 | 17.85 | 0.07 |
| 55962.2 | 17.93 | 0.07 |
| 55983.2 | 17.80 | 0.23 |
| 56166.5 | 18.01 | 0.09 |
| 56168.5 | 18.13 | 0.07 |
| 56169.5 | 17.97 | 0.08 |
| 56170.5 | 18.03 | 0.06 |
| 56173.5 | 18.19 | 0.08 |
| 56174.5 | 18.00 | 0.08 |
| 56177.5 | 18.27 | 0.17 |
| 56178.5 | 18.09 | 0.09 |
| 56179.5 | 18.16 | 0.11 |
| 56182.5 | 18.07 | 0.07 |
| 56184.5 | 18.10 | 0.09 |
| 56189.5 | 18.14 | 0.08 |
| 56190.5 | 18.08 | 0.05 |
| 56191.4 | 18.05 | 0.07 |
| 56194.5 | 18.09 | 0.06 |
| 56198.4 | 18.04 | 0.08 |
| 56200.5 | 18.12 | 0.13 |
| 56201.5 | 18.12 | 0.16 |
| 56203.4 | 18.09 | 0.08 |
| 56207.4 | 17.99 | 0.08 |
| 56208.5 | 18.02 | 0.08 |
| 56214.5 | 17.98 | 0.04 |
| 56215.4 | 18.00 | 0.07 |
| 56218.5 | 18.01 | 0.07 |
| 56219.4 | 18.16 | 0.09 |
| 56220.4 | 18.12 | 0.06 |
| 56224.5 | 18.11 | 0.17 |
| 56228.3 | 17.98 | 0.11 |

Table 1 – *continued* Unfiltered KAIT Photometry of UGC 2773-OT

| MJD | mag | 1σ (mag) |
|---------|-------|-----------------|
| 56309.1 | 18.24 | 0.11 |
| 56312.1 | 17.99 | 0.09 |
| 56527.5 | 18.25 | 0.08 |
| 56533.5 | 18.18 | 0.12 |
| 56535.5 | 18.13 | 0.15 |
| 56540.5 | 18.15 | 0.09 |
| 56547.5 | 18.19 | 0.10 |
| 56548.5 | 18.13 | 0.10 |
| 56549.5 | 18.15 | 0.06 |
| 56552.4 | 18.28 | 0.16 |
| 56554.4 | 18.19 | 0.16 |
| 56558.4 | 18.20 | 0.09 |
| 56561.4 | 18.19 | 0.13 |
| 56563.5 | 18.27 | 0.09 |
| 56567.4 | 18.44 | 0.13 |
| 56570.5 | 18.20 | 0.07 |
| 56571.4 | 18.12 | 0.11 |
| 56573.4 | 18.28 | 0.07 |
| 56579.4 | 18.08 | 0.09 |
| 56581.4 | 18.36 | 0.14 |
| 56583.4 | 18.44 | 0.13 |
| 56588.4 | 18.36 | 0.07 |
| 56590.5 | 18.16 | 0.21 |
| 56592.4 | 18.12 | 0.07 |
| 56598.4 | 18.29 | 0.07 |
| 56601.4 | 18.18 | 0.10 |
| 56603.4 | 18.54 | 0.37 |
| 56605.5 | 18.06 | 0.08 |
| 56610.2 | 18.16 | 0.14 |
| 56612.3 | 18.27 | 0.14 |
| 56620.4 | 18.17 | 0.09 |
| 56625.3 | 18.47 | 0.11 |
| 56627.3 | 18.35 | 0.13 |
| 56636.3 | 18.27 | 0.10 |
| 56639.2 | 18.33 | 0.11 |
| 56668.2 | 18.07 | 0.13 |
| 56679.2 | 18.21 | 0.08 |
| 56682.2 | 18.29 | 0.08 |
| 56883.5 | 18.54 | 0.22 |
| 56893.4 | 18.42 | 0.06 |
| 56893.5 | 18.49 | 0.08 |
| 56895.5 | 18.40 | 0.05 |
| 56896.5 | 18.47 | 0.05 |
| 56898.5 | 18.44 | 0.05 |
| 56903.5 | 18.54 | 0.10 |

sion of the fact that most aspects of the traditional view of LBVs (HD94) have not stood the test of time. Continued study has shown that rigid imposition of definitions of LBVs (HD94) have not been supported by detailed analysis on several fronts, and these definitions would in fact exclude most LBVs from the class. In particular, the important conjecture that S Dor variations are caused by optically thick winds at constant L_{Bol} may be wrong, and steady super-Eddington winds may not be the correct or dominant driving mechanism in many giant LBV eruptions (see review by Smith 2014).

Studies with quantitative spectroscopy (de Koter et al. 1996; Groh et al. 2009a,b) have disproven the conjecture that S Dor brightening events are caused by developing pseudo-photospheres in optically thick winds (Davidson 1987, HD94). The mass-loss rates of S Dor maxima are not high enough to make such large pseudo-photospheres, and so they are more likely to be caused by envelope inflation or pulsation (Graefner et al. 2012). Moreover, bolometric luminosities during S Dor eruptions are not really constant (Groh et al. 2009a). Similarly, the idea that giant-

eruption maxima are caused by pseudo-photospheres in opaque super-Eddington winds is challenged by light-echo spectra of η Carinae (Rest et al. 2012; Prieto et al. 2014), by detailed analysis of the ejecta around η Car that are better matched by explosive models (Smith et al. 2003; Smith 2006, 2008), and the fact that many extragalactic giant LBV eruptions are relatively hot at peak luminosity rather than cool (Smith et al. 2011; Mauerhan et al. 2015). Last, as discussed by Smith & Tombleson (2015), the central paradigm of the role that LBVs play in stellar evolution and their connection to stars with the highest initial masses is probably incorrect, because their isolation from massive O-type stars dictates that they are largely products of binary evolution and not a transitional state in the lives of the most massive stars. There are many ways in which violent binary interaction may be important for understanding LBVs and related transients (Soker 2001; Podsiadlowski 2010; Kochanek et al. 2014; Smith & Tombleson 2015; Smith 2014).

In any case, it is perhaps sufficient to state that our understanding of LBVs, LBV giant eruptions, shells around nearby LBVs, and extragalactic SN impostors is still too poor to make broad generalizations about the nature of the SN impostors or their connection to LBVs. The number of well-studied objects is still very small, and a close look at the physical properties of additional examples is quite valuable. Much of our interpretation of these events is coloured by the vast amount and quality of data for η Car that far surpasses all other cases, making comparisons tempting but sketchy. Finding extragalactic analogs that actually match η Car has so far been difficult.

In this paper we present an update on the ongoing outburst of the LBV-like transient UGC 2773-OT. The “update” refers to developments since our first paper on this object (Smith et al. 2010), which discussed photometry and spectra obtained shortly after the time of discovery, as well as archival data that showed a relatively faint progenitor 10 years before discovery and a gradual brightening for 5 yr before (see below). In that paper, we found that the transient had a relatively cool spectrum (~ 7000 K) and relatively slow outflow speeds ($200\text{--}300$ km s $^{-1}$), a mild IR excess from circumstellar dust, and a luminous yellow progenitor with $\log(L/L_{\odot}) = 5.1$ (although it could have been substantially hotter and more luminous, due to possible foreground extinction from circumstellar dust). The likely effective initial mass indicated by comparing the quiescent progenitor to single-star models was found to be $\gtrsim 20$ M $_{\odot}$ (more if additional extinction was significant or if the star was hot). Foley et al. (2011) presented additional complementary spectra of UGC 2773-OT, and came to similar conclusions about its physical properties and LBV-like nature. In the time since these first papers, UGC 2773-OT has continued to evolve slowly, declining from its peak but remaining at relatively high outburst luminosity. If the progenitor really was an initially 20 M $_{\odot}$ star, then the transient has exceeded the classical Eddington luminosity for more than a decade. The fact that it has persisted for a decade in this high-luminosity state is physically meaningful, as discussed in this paper. In this sense, we suggest that it is so far the only known example of an extragalactic SN impostor that behaves similar to the 19th century Great Eruption of η Carinae. This extends the comparison made by Rest et al. (2012), who remarked that spectra of UGC 2773-OT ob-

tained shortly after discovery provided the closest match among known SN impostors to the low-temperature spectra of η Car’s light echoes. In this paper we report changes in the spectrum of UGC 2773-OT after several years, and it will be interesting to see if η Car’s light echoes develop similar changes as time passes.

UGC 2773-OT was observed to occur in the central parts of the dwarf irregular galaxy UGC 2773, and its brightening was discovered (Boles et al. 2009) on 2009 August 18.08 (UT dates are used throughout this paper). As in our previous paper (Smith et al. 2010), we adopt $m - M = 28.82$ mag, $E(B - V) = 0.56$ mag, and $A_R = 1.51$ mag for the Milky Way reddening and extinction in the line of sight to the host galaxy UGC 2773, and we refer to day 0 as the date of discovery. We present new photometry and spectra in Section 2, and we combine these with our previously published photometry and spectra. In Section 3 we summarise the observational results, and in Section 4 we discuss physical interpretations in context with other LBVs — especially one of them.

2 OBSERVATIONS

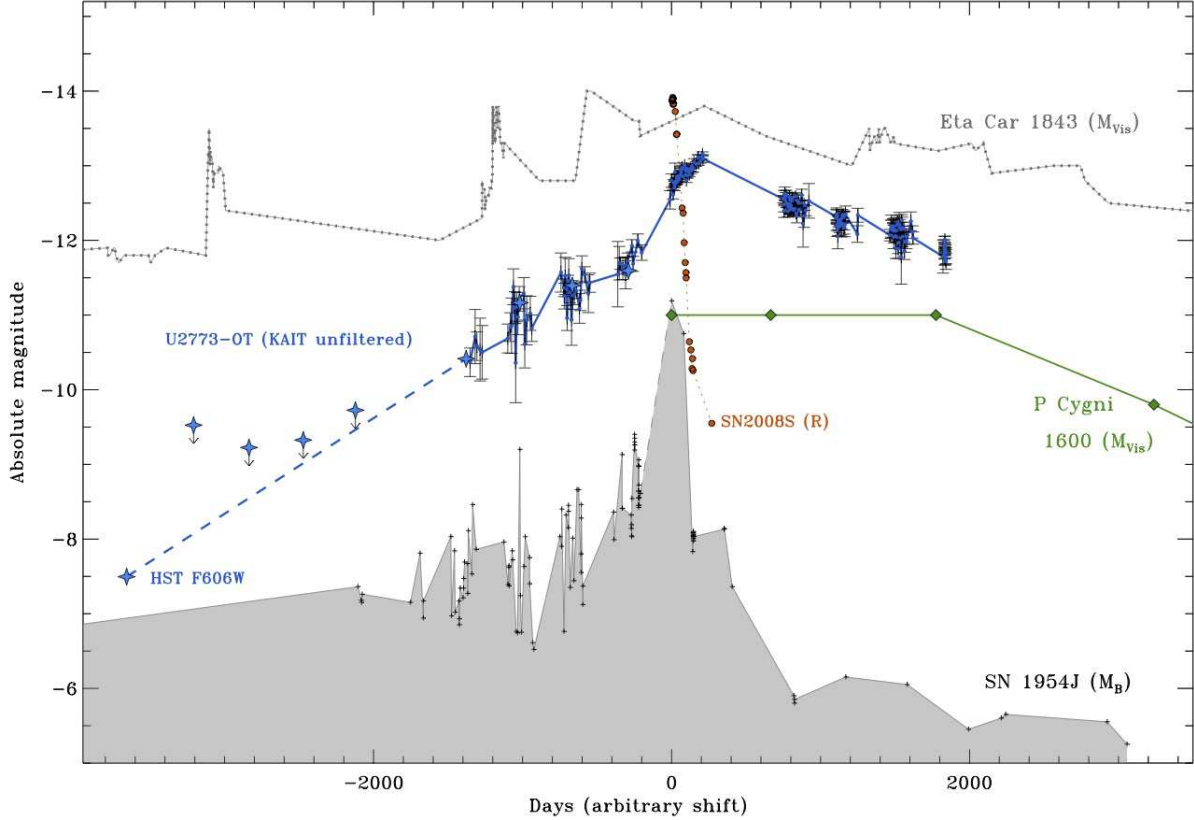
2.1 KAIT Photometry

UGC 2773, the dwarf irregular host galaxy of UGC 2773-OT, has been monitored regularly with the Katzman Automatic Imaging Telescope (KAIT; Filippenko 2003) at Lick Observatory. As demonstrated by Li et al. (2002), the best match to broadband filters for the KAIT unfiltered data is the R band (although note that bright H α line emission will influence the R band more than the unfiltered data). We list the KAIT apparent unfiltered magnitudes of UGC 2773-OT in Table 1, and the apparent magnitudes are plotted in Figure 1. This table lists only KAIT observations since the time of discovery. We analyzed predisccovery unfiltered images and detected a source at the position of UGC 2773-OT during the ~ 5 yr before discovery, as well as upper limits before that. There were multiple observations each year, so we produced stacked seasonal averages to improve the sensitivity. Further information about the predisccovery photometry is available in our previous paper (Smith et al. 2010). A stacked image from the year 2000, when UGC 2773-OT was not detected, is used as a template image in an image-subtraction technique to cleanly remove the galaxy contamination at the position of UGC 2773-OT in later images. This is important because UGC 2773-OT is in a crowded region of its host, and so we may expect different results from template-subtracted photometry and raw aperture photometry. The photometry listed here is a reduction and analysis of the same data from 2009 that were published earlier, plus new observations since 2009. Unfortunately, KAIT observations of UGC 2773-OT during the 2010 season are not available because of a failure in the data storage device, so there is a gap in the light curve 1 yr after discovery.

To put the flux on an absolute magnitude scale, we adopt the same distance and reddening from our previous study (Smith et al. 2010), and listed here in the Introduction. The resulting absolute magnitude light curve is shown in Figure 2, along with some other transient sources from the literature for comparison.

Table 2. Visible and IR Photometry

| Date | JD | <i>B</i> | 1 σ | <i>V</i> | 1 σ | <i>R</i> | 1 σ | <i>I</i> | 1 σ | <i>J</i> | 1 σ | <i>H</i> | 1 σ | <i>K</i> | 1 σ |
|----------|---------|----------|------------|----------|------------|----------|------------|----------|------------|----------|------------|----------|------------|----------|------------|
| 8/19/14 | 2456883 | ... | ... | ... | ... | ... | ... | ... | ... | 17.36 | 0.07 | 17.07 | 0.07 | 16.48 | 0.09 |
| 10/16/14 | 2456946 | 20.00 | 0.14 | ... | ... | 18.05 | 0.07 | 17.86 | 0.08 | ... | ... | ... | ... | ... | ... |
| 11/16/14 | 2456977 | 19.87 | 0.26 | 18.68 | 0.08 | 18.17 | 0.07 | 17.66 | 0.13 | ... | ... | ... | ... | ... | ... |
| 11/29/14 | 2456990 | 19.38 | 0.14 | 18.78 | 0.05 | 18.05 | 0.05 | 17.61 | 0.12 | ... | ... | ... | ... | ... | ... |
| 12/28/14 | 2457019 | ... | ... | 18.82 | 0.09 | 18.10 | 0.11 | 17.77 | 0.12 | ... | ... | ... | ... | ... | ... |
| 1/11/15 | 2457033 | ... | ... | ... | ... | ... | ... | ... | ... | 17.10 | 0.09 | 16.79 | 0.10 | ... | ... |
| 1/21/15 | 2457043 | ... | ... | ... | ... | ... | ... | ... | ... | 17.11 | 0.07 | 16.82 | 0.09 | ... | ... |
| 1/29/15 | 2457051 | ... | ... | ... | ... | ... | ... | ... | ... | ... | ... | ... | ... | 16.28 | 0.1 |
| 2/10/15 | 2457063 | 19.86 | 0.15 | 18.67 | 0.09 | 18.06 | 0.07 | 17.86 | 0.17 | ... | ... | ... | ... | ... | ... |

**Figure 2.** The absolute magnitude light curve of UGC 2773-OT compared to those of other transients: η Car’s 19th century eruption (Smith & Frew 2011), P Cyg’s 1600 AD eruption (Smith et al. 2015, in prep.), and the brief SN impostor SN 2008S (Smith et al. 2009a).

2.2 Visible/IR Photometry

Johnson *B*, *V*, Harris *R*, and Arizona *I* band imaging was obtained with the Mont4k instrument mounted on the 1.55m Kuiper telescope located on Mt. Bigelow, Arizona. Observations were taken on 2014 October 16, November 16, 29, and December 28, and on 2015 February 10 in 3×3 binning mode, resulting in a final pixel scale of $0''.43$. The observations were then reduced and combined into final images using standard IRAF *ccdred* procedures and dome flats.

NIR imaging observations were taken with the 3.8-m United Kingdom Infrared Telescope (UKIRT) on Mauna Kea using UFTI (2014 August 19) and WFCAM2 (2015 January 11, 21, and 29). *JHK* observations were pipeline reduced by the Cambridge Astronomical Survey Unit (CASU).

Aperture photometry was performed on all images using a $1''.3$ aperture to mitigate contamination from adjacent

host galaxy light, and was calibrated using APASS optical and 2MASS NIR standard stars present in the field. *R* and *I* band standards were transformed from APASS *r* and *i* magnitudes using Jester et al. (2005). For both optical and NIR data, uncertainties were calculated by adding in quadrature photon statistics and zero point deviation of the standard stars for each epoch. The resulting photometry is listed in Table 2.

2.3 Spectra

We obtained several epochs of optical spectroscopy of UGC 2773-OT using a number of different facilities over the past 6 years, including the Bluechannel (BC) spectrograph on the 6.5-m Multiple Mirror Telescope (MMT), the Boller & Chivens (B&C) Spectrograph mounted on the 2.3-

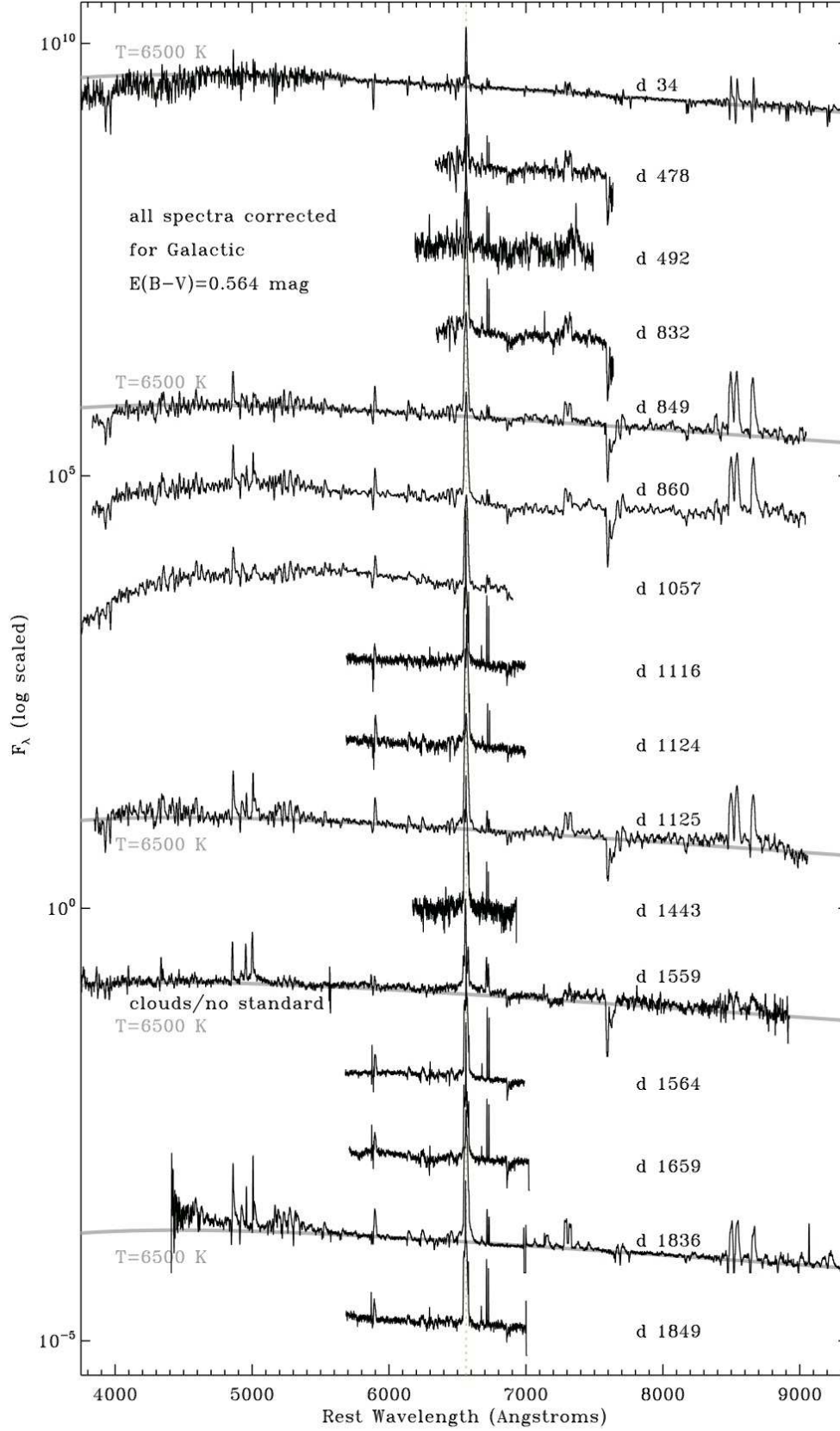


Figure 3. Visible-wavelength spectra of UGC 2773-OT obtained with the Keck, MMT, and Bok telescopes over the past 6 years (see Table 3). As noted in the figure, all spectra shown here have been corrected for the Milky Way line-of-sight reddening.

Table 3. Log of Spectroscopic Observations

| UT date | day ^a | Tel./Instr. | $\Delta\lambda(\text{\AA})$ | Comment |
|-------------|------------------|-------------|-----------------------------|------------------|
| 2009 Sep 22 | 34 | Keck/LRIS | 3600-9200 | Paper I, low res |
| 2009 Sep 22 | 34 | Keck/LRIS | 3800-5100 | Paper I, hi res |
| 2009 Sep 22 | 34 | Keck/LRIS | 6250-7850 | Paper I, hi res |
| 2011 Jan 13 | 478 | MMT/BCh | 6345-7640 | 1200 lpm |
| 2011 Jan 14 | 479 | MMT/BCh | 6345-7640 | 1200 lpm |
| 2011 Jun 27 | 492 | MMT/BCh | 6200-7490 | 1200 lpm |
| 2012 Jan 03 | 832 | MMT/BCh | 6350-7645 | 1200 lpm |
| 2012 Jan 20 | 849 | MMT/BCh | 3850-9050 | 300 lpm |
| 2012 Jan 31 | 860 | MMT/BCh | 3850-9050 | 300 lpm |
| 2012 Aug 14 | 1057 | Bok/BC | 3610-6900 | low res |
| 2012 Oct 16 | 1116 | MMT/BCh | 5700-7000 | 1200 lpm |
| 2012 Nov 24 | 1124 | MMT/BCh | 5700-7000 | 1200 lpm |
| 2012 Nov 25 | 1125 | MMT/BCh | 3850-9050 | 300 lpm |
| 2013 Sep 04 | 1443 | MMT/BCh | 5700-7000 | 1200 lpm |
| 2013 Dec 29 | 1559 | MMT/BCh | 3850-9050 | 300 lpm |
| 2014 Jan 03 | 1564 | MMT/BCh | 5700-7000 | 1200 lpm |
| 2014 Apr 08 | 1659 | MMT/BCh | 5700-7000 | 1200 lpm |
| 2014 Oct 02 | 1836 | Keck/DEIMOS | 4410-9640 | low res |
| 2014 Oct 15 | 1849 | MMT/BCh | 5700-7000 | 1200 lpm |
| 2015 Mar 22 | 2007 | MMT/BCh | 5700-7000 | 1200 lpm |

^aRelative to discovery (as in Paper I).

m Bok telescope on Kitt Peak, the Low-Resolution Imaging Spectrometer (LRIS; Oke et al. 1995) mounted on the 10-m Keck I telescope, and the Deep Imaging Multi-Object Spectrograph (DEIMOS; Faber et al. 2003) on Keck II. Details of the spectral observations are summarised in Table 3. For MMT spectra, we either used the 1200 lpm grating (moderately high resolution) or the 300 lpm grating (low resolution). The slit was always oriented at the parallactic angle (Filippenko 1982), and the long-slit spectra were reduced using standard procedures. Final spectra are shown in Figure 3, including the first epoch of spectra, which is from our previous paper (Smith et al. 2010). Several epochs in Figure 3 have a blackbody plotted in grey; these are intended only as a rough relative comparison. Nevertheless, inferred temperatures around 6500 K suggest that these quoted temperatures are not wildly in error. Details of the $H\alpha$ line profile are shown in Figure 4, $H\beta$ is shown in Figure 5, details of the region around Na I D and He I $\lambda 5876$ are shown in Figure 6, and Fe II $\lambda\lambda 6148, 6149$ is shown in Figure 7.

3 RESULTS

3.1 Light Curve

In our previous study (Smith et al. 2010), we showed that predisccovery photometry of UGC 2773-OT showed a slow and steady brightening in the 5 yr prior, when it was 3 or more magnitudes brighter than its quiescent progenitor detected a decade before discovery in *HST* images (the predisccovery brightening is reproduced in Figure 2). As noted earlier (Smith et al. 2010; Foley et al. 2011), the *HST* data for the progenitor correspond to a star of at least $\sim 20 M_{\odot}$ and $\log(L/L_{\odot}) = 5.1$. Those authors both noted, however, that these estimates for the progenitor are likely to be just lower limits because with a small amount of circumstellar dust extinction (motivated by the early IR excess), the progenitor could easily be hotter and more luminous, corresponding to a 40–60 M_{\odot} star or more. Thus, the slow brightening in the years before discovery could have been partially due to colour evolution from a hot to a cooler state, in addition

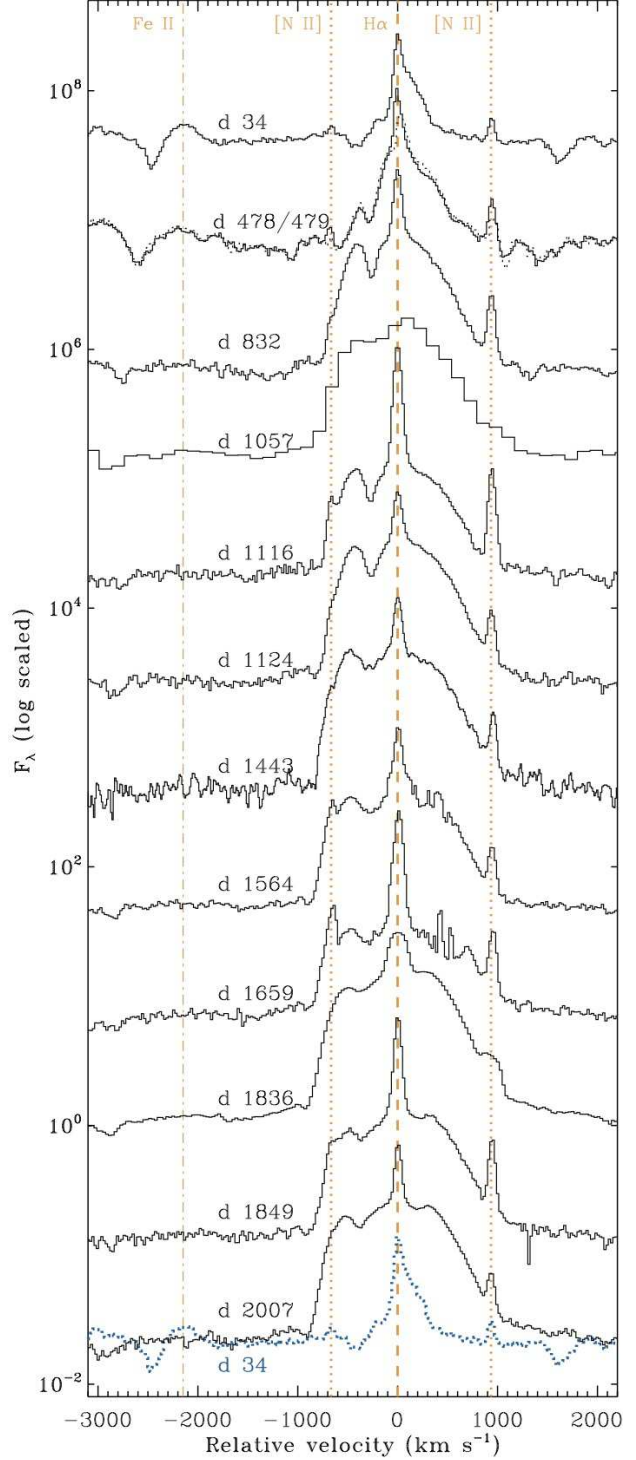


Figure 4. The $H\alpha$ line profile as seen in our spectra of UGC 2773-OT. Narrow emission components of [N II] and $H\alpha$ that are probably associated with an underlying H II region or distant CSM are indicated by the orange vertical lines through the figure. An orange vertical line also notes the location of an Fe II line. The first-epoch spectrum (day 34) is reproduced at the bottom of the plot in a dashed-blue tracing for comparison with the latest epochs.

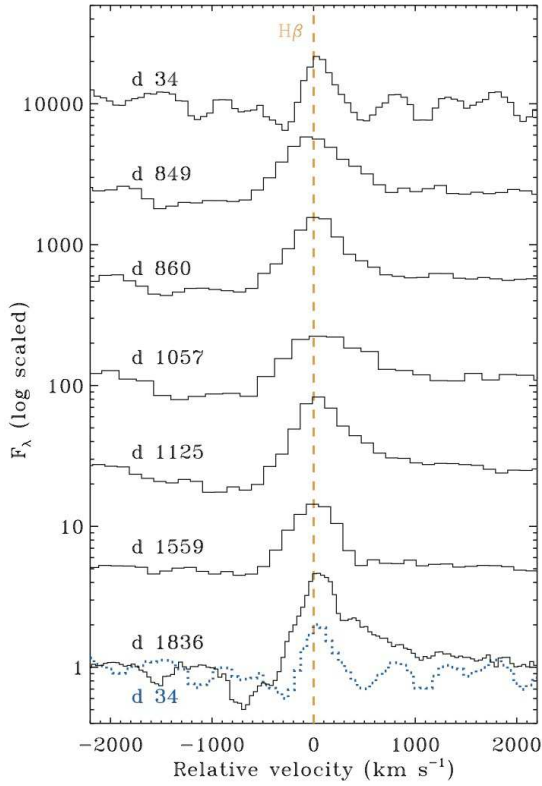


Figure 5. Same as Figure 4, but for H β . Our spectral dataset includes fewer epochs that sample H β , and only with low-resolution spectra that cover a broader wavelength range.

to a real increase in bolometric luminosity. Unfortunately, information about the prediscovery colour evolution is not available aside from the single *HST* epoch.

Since reaching its peak apparent brightness around day 200 (as plotted in Figure 2) until day ~ 2000 , UGC 2773-OT has had a very slow and steady decline rate at visible wavelengths. There may be small fluctuations in brightness, but the overall trend appears smooth. From the KAIT light curve, we measure an average decline rate of 0.26 mag yr^{-1} during the first ~ 2000 days.

There is very little colour evolution during this slow decline, and the trend is toward slightly bluer colours at late times. In the inset of Figure 1, we show the spectral energy distribution (SED) for early times around days 20–40, as well as late times around day 2000. The early-time photometry include IR *JHK* magnitudes from our previous study (Smith et al. 2010) and *gri* magnitudes from Foley et al. (2011) taken at the same epoch, both dereddened by $E(B - V) = 0.56 \text{ mag}$. The optical/IR SED at early times can be approximated with a $\sim 6500 \text{ K}$ blackbody, which is consistent with our low-resolution spectrum on day 34 shown in Figure 3. At later times, the SED indicates a slightly warmer temperature, but as we discussed below, this is mostly due to a combination of a continuum photosphere at about the same temperature, plus a blue excess from emission lines.

Neither early nor late epochs show a substantial IR excess. At early times, one could deduce a small near-IR excess by choosing a slightly warmer characteristic temperature for

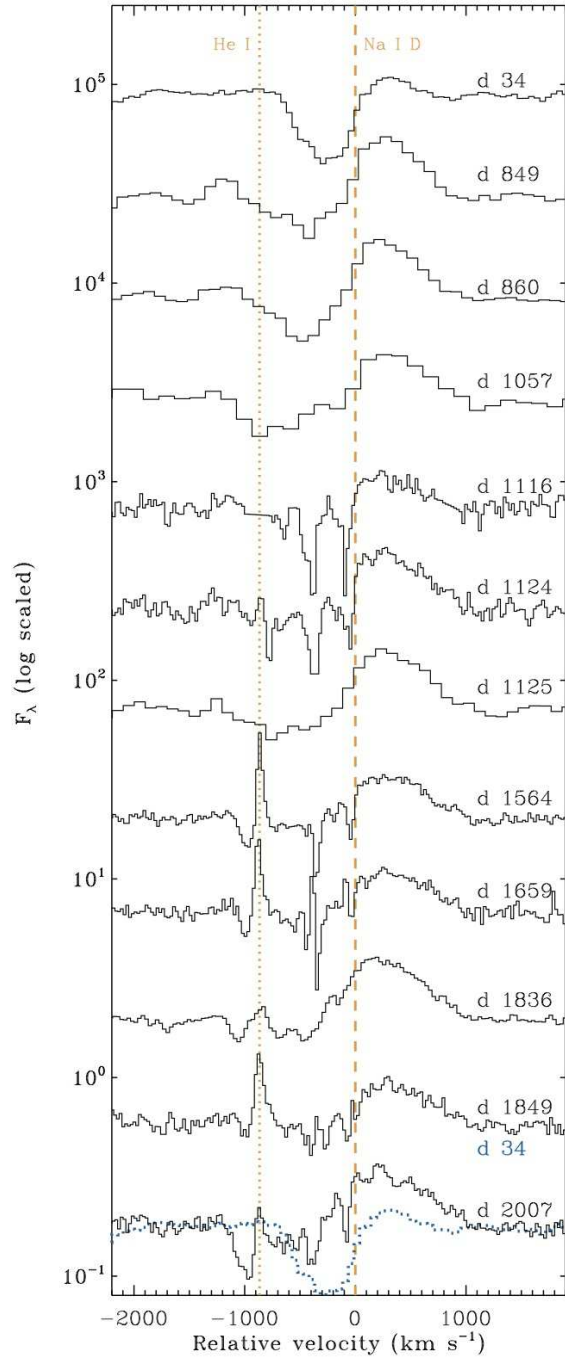


Figure 6. Line profiles of Na I D (at $v=0 \text{ km s}^{-1}$) and He I $\lambda 5876$ as seen in our spectra of UGC 2773-OT. The first epoch spectrum (day 34) is reproduced at the bottom of the plot in a dashed blue tracing for comparison with the latest epochs.

optical data plus a small amount of hot dust to match the IR fluxes (Foley et al. 2011; Smith et al. 2010). At late epochs, the *J* and *H* magnitudes are consistent with an extension of the optical blackbody, but there does appear to be a small *K*-band excess. This may be due to the formation of new dust, cooling of CSM dust heated by an IR echo, or the destruction of the hottest dust seen previously, leaving the cooler dust at larger radii. Continued monitoring of the IR fluxes may be interesting; if UGC2773-OT fades as η Car-

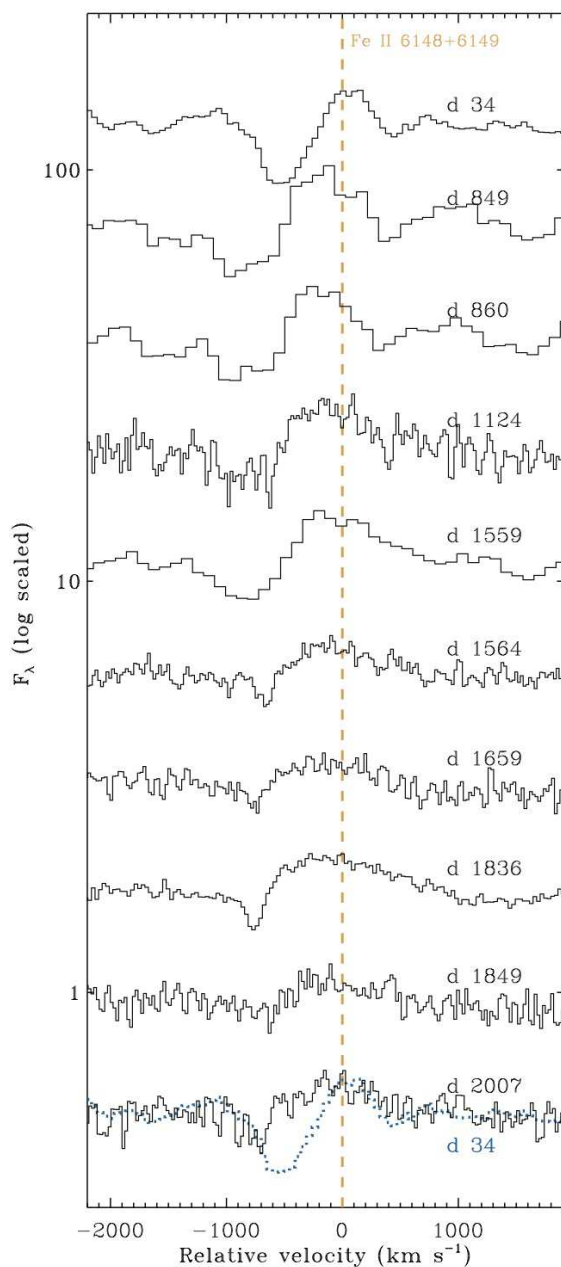


Figure 7. The Fe II $\lambda\lambda 6148,6149$ line profile as seen in our spectra of UGC 2773-OT. The first epoch spectrum (day 34) is reproduced at the bottom of the plot in a dashed blue tracing for comparison with the latest epochs.

nae did at the end of its decade-long plateau, we may see a strong increase in the IR excess.

Although there has been only gradual change in the light curve of UGC 2773-OT over the past few years, there have been some pronounced changes in its spectrum, as discussed next.

3.2 Spectroscopy

In our previously reported day 34 spectrum (Smith et al. 2010) obtained shortly after discovery and near the time of peak luminosity, UGC 2773-OT showed a cool absorption-

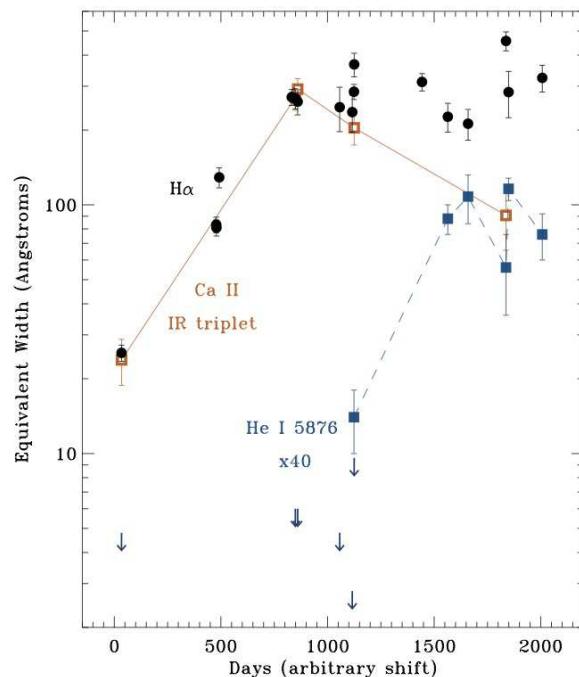


Figure 8. Measured emission-line EWs (emission is positive) of $H\alpha$ as compared to the EWs for the Ca II IR triplet and He I $\lambda 5876$. $H\alpha$ (black filled points) was integrated from roughly -1200 to $+1800$ km s^{-1} , and the uncertainty is dominated by signal to noise of the continuum. For Ca II (orange unfilled squares, connected by orange lines), we took the integrated EW of all 3 lines, and so P Cygni absorption at some epochs weakens the emission EW. The relatively wide continuum also raises the EW uncertainty due to the choice of the continuum level. For He I $\lambda 5876$ (blue squares and arrows) we have only upper limits at early times determined by the signal to noise ratio of the spectra, whereas we clearly detect narrow He I at later times, although at those epochs we sometimes also see an accompanying P Cygni absorption that adds to uncertainty in choosing a continuum level. (We did not use the day 1559 spectrum, which suffered from calibration problems due to weather.) The He I EW is multiplied by a factor of 40 for display.

line spectrum, similar to late F-type or G-type supergiants, and similar in some ways to the spectra of LBVs in their cool state. Foley et al. (2011) presented similar spectra of UGC 2773-OT obtained around the same epoch. The early spectrum was characterised by heavy line blanketing by numerous narrow absorption lines in the blue, and relatively weak and narrow $H\alpha$ emission. An echelle spectrum taken with Keck/HIRES on day 22 showed a clear P Cygni profile in $H\alpha$ that suggested outflow speeds around 360 km s^{-1} (Smith et al. 2010). The early spectrum showed strong absorption from Ca II H and K, very weak emission in the forbidden [Ca II] doublet, and a relatively weak P Cygni profile in the Ca II IR triplet (Smith et al. 2010). These are similar to the spectral properties seen in SN 2008S-like objects (Prieto 2008; Prieto et al. 2008a; Thompson et al. 2009). Subsequently, Rest et al. (2012) showed that our day 34 spectrum of UGC 2773-OT resembled spectra of light echoes from η Carinae, also thought to correspond to early phases in its historical giant LBV eruption near peak.

In the intervening ~ 6 yr, the spectrum of UGC 2773-OT has shown gradual and subtle changes as the source

faded slowly. The overall spectral evolution is shown in Figure 3. While the visible/red continuum slope has remained roughly constant at a characteristic apparent temperature around 6500 K, there are a number of other changes reminiscent of increasing temperature/ionization or dropping optical depth. The forest of narrow absorption lines that cause strong line blanketing in the blue (day 34) weakened considerably, and many narrow features including numerous Fe II lines change into emission rather than absorption; this is discussed more below. We see weakening and disappearing P Cygni absorption features, and strengthening with time of emission components of Balmer lines and the Ca II triplet. Later epochs even show narrow He I in emission, which is absent at early epochs. One of the most pronounced changes is seen in the H α profile, which becomes stronger, broader, and develops an asymmetric and irregular profile (Figure 4). Implications of the H α profile are discussed later.³

An interesting comparison involves the relative strengths of H α , the Ca II IR triplet, and He I λ 5876. The time dependence of equivalent widths (EWs) for these three lines is plotted in Figure 8. While the light curve shows only gradual fading of about 1.5 mag (a factor of 4) in \sim 2000 days, the H α EW climbs by a factor of \sim 150 or more, so these changes in EW also trace changes in line luminosity.⁴

Underscoring the unusual changes to H α , the H β line does not show a similar evolution in terms of its profile shape or relative strength. On day 34, the H α /H β flux ratio is 7.7 ± 1 (not corrected for any local reddening), and the H α /H β flux ratio then climbs to 31 ± 2 by day 1057. This indicates that H β does not increase in strength as much as H α , probably signifying a growing contribution from shock excitation at later times. This increasing H α /H β ratio is not due to increased reddening from dust, since the continuum shows basically no change in slope, while H α develops a line profile that is very different from H β . Also, the profile of H β retains its P Cyg absorption, whereas H α goes fully into emission with an asymmetric profile. Interestingly, though, the speed of the H β P Cygni trough increases from around 300 km s⁻¹ on day 34 to about 700–800 km s⁻¹ by day 1836 (Figure 5). An important point is that at each epoch, the blue P Cygni absorption in H β is at a similar speed to the blue emission bump seen in H α . Thus, both H β and H α trace a dramatic increase in outflow speed with time during the event. If the outflow speed is increasing with time, the fast material must catch up with and overtake the slower

³ Since our spectra were obtained at epochs that still trace relatively high densities in the outflow, forbidden lines that one normally uses to study abundances are mostly quashed (and would be difficult to separate from a surrounding H II region anyway), so we do not provide a discussion of the CNO composition of UGC 2773-OT for comparison with η Car (Davidson et al. 1986; Smith & Morse 2004).

⁴ In fact, a high resolution spectrum on day 22 (Smith et al. 2010) shows that more than 2/3 of the early time H α EW we measure is actually due to narrow H α and [N II] from an unresolved H II region, whereas the H II region contributes a much lower fraction at late times because the broad component has strengthened. The true relative increase in H α strength is therefore even larger than indicated in Figure 8 by another factor of 2–3.

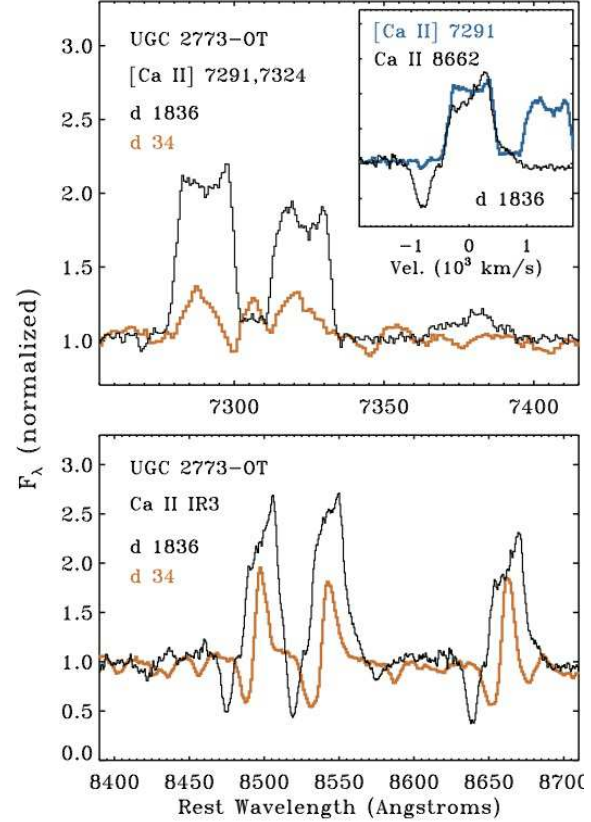


Figure 9. A comparison of the early and late-time spectra for UGC 2773-OT, highlighting the red Ca⁺ lines. The top panel shows the [Ca II] $\lambda\lambda$ 7291,7324 doublet on days 34 (black) and 1836 (orange), while the bottom panel shows the same two dates for the Ca II IR triplet at 8498, 8542, and 8662 Å. Both sets of lines show an increase in strength, and the P Cygni absorption of the Ca II IR triplet shows an unambiguous increase in velocity. The inset in the upper right shows the line profile shapes as a function of rest-frame velocity for [Ca II] $\lambda\lambda$ 7291 (blue) and Ca II λ 8662 (black).

material ejected earlier, indicating that shocks should play an important role in the event. This is discussed more below.

The EW of the Ca II IR triplet increases in-step with H α for the first 1000 days, but while H α levels off for the next 1000 days, Ca II fades by more than a factor of 3. At around the same time, He I λ 5876 transitions from non-detection in the first 1000 days, to then rising as Ca II falls (note that the He I EW is multiplied by a factor of 40 for display in Figure 8). Thus, the changes after day 1000 likely indicate a rise in ionization and electron temperature (especially He I emission, but also Ca⁺ getting partly ionized to Ca⁺⁺) that accompanies a falling optical depth. The likely physical significance of these changes is discussed below in Section 4.1.

The behavior of the red/IR lines of Ca⁺ are particularly interesting, and are relevant to comparisons with other types of SN impostors and η Car. Figure 9 illustrates the changes in line intensity and profile shape with time. This figure shows the day 34 (near peak) and day 1836 spectra of the [Ca II] $\lambda\lambda$ 7291,7324 doublet and the Ca II IR triplet at 8498, 8542, and 8662 Å. Both sets of lines increase in strength (in accord with Figure 8), but the increase in [Ca II]

emission flux is more dramatic because these lines were very weak on day 34. This increase is similar to the increase in [Ca II] emission strength seen in light echoes of η Car as it faded (Prieto et al. 2014). The velocity profiles of the lines also change markedly between the two epochs. The [Ca II] lines develop a boxy or even double-peaked profile, with a FWHM of $821(\pm 5)$ km s $^{-1}$, and with the line wings dropping steeply to the continuum level at $-530 (\pm 15)$ and $+530 (\pm 15)$ km s $^{-1}$. Thus, the emission is narrower than the broad asymmetric emission profile of H α at late epochs (Figure 4). The Ca II IR triplet lines show the same boxy emission profile with almost exactly the same width (see the inset in Figure 9), but the tops of the profiles are skewed to the red, presumably because of some blueshifted self-absorption that diminishes the blue peak. The Ca II IR triplet lines also have blueshifted P Cygni absorption components, with the velocity of the absorption trough minimum increasing dramatically from $-350 (\pm 30)$ km s $^{-1}$ on day 34 to $-800 (\pm 20)$ km s $^{-1}$ on day 1836. The velocity of the Ca II P Cygni absorption is therefore similar to the speed of the blue bump in the H α emission profile at late times. The Ca+ emission components do not trace this faster material, and therefore originate from a different zone in the outflow; this may be relevant for interpretations of the [Ca II] emission in other SN impostors, like the SN 2008S-like objects mentioned in the Introduction, as well as the [Ca II] emission seen in light echoes of η Carinae, which have been compared to UGC 2773-OT (Rest et al. 2012; Prieto et al. 2014). The geometry of the outflow is discussed below in Section 4.2.

4 DISCUSSION

4.1 Wind/ejecta vs. Shock Interaction

While the light curve of UGC 2773-OT shows a very gradual rate of fading, there are interesting spectroscopic changes over the past 6 years that hold important clues about the physical processes in the eruption. Overall, the observed spectrum held an almost constant continuum temperature at 6500 K while fading about 1.5 mag in visible light. Despite the unchanging observed continuum slope, there are signs of increasing ionization and excitation that seem inconsistent with this relatively low and constant apparent continuum temperature. The early time spectra around peak apparent brightness are qualitatively consistent with expectations for either a cool optically thick wind, or a photosphere that is formed in the expanding ejecta of an explosion. As time proceeds, however, we begin to see clear signs that a strong shock wave is contributing to the spectrum. This spectral evolution therefore gets to the crux of a key current question regarding LBV eruptions (see Smith et al. 2011): are they driven by super-Eddington winds or hydrodynamic explosions? While we cannot claim from available evidence that a super-Eddington wind (Owocki et al. 2004) plays no role in lifting material from the star (in fact it may help produce the CSM into which the explosion crashes), there are several lines of evidence that point to or require strong shock excitation as playing a key role in powering the event, especially at later times. These are:

1. In the past 6 years, H α has increased sharply in EW and line luminosity in UGC 2773-OT, as seen in the normal

evolution of SNe IIn powered largely or entirely by CSM interaction. Also, the H α /H β ratio increases as the H α luminosity climbs. This increasing flux ratio favours collisional excitation in a shock rather than photoionization and recombination as the power source for the strong H α emission. Again, late-time spectra of SNe IIn exhibit very strong H α , often with little else detected in their visible-wavelength spectra.

2. The EW and line flux of He I $\lambda 5876$ strengthens after day 1000, even though the apparent continuum temperature changes little. A 6500 K photosphere cannot photoionize a substantial fraction of the He to produce He I recombination emission. This requires an additional source of high excitation. Interestingly, the Ca II IR triplet weakens as the He I $\lambda 5876$ EW strengthens, while H α remains strong after day 1000 (Fig. 8). This again suggests an increase in ionization from Ca $^+$ to Ca $^{++}$. A significant change in ionization is not expected for photoexcitation alone if the apparent continuum temperature is unchanged. He I $\lambda 5876$ emission generally would require temperatures above 20,000 K. The excess ionization is likely due to X-rays and far-UV radiation from a shock.

3. Characteristic outflow speeds are increasing with time, as seen in the increased width of the H α emission profile as well as the increasing speed of the blueshifted P Cygni absorption trough of H β (from about 300 to 800 km s $^{-1}$) and Ca II. If the outflow speed is increasing, one expects that fast ejecta must catch up with slow material ejected previously, giving rise to a shock.

4. The blue portion of the visible spectrum changed from a forest of narrow absorption lines at early times indicative of the strong line-blanketing seen in dense winds and cooling ejecta (day 34) to an excess of blue emission lines at later epochs. Figure 10 directly compares the day 34 spectrum with strong blue line blanketing to the day 1836 spectrum with excess blue emission, with both spectra normalised to the red continuum level. While their red spectra are very similar (except for the strength of H α and a few other individual lines), the spectra at these two epochs are very different in the blue. To isolate the *excess* blue emission, the bottom panel in Figure 10 shows a spectrum of the residual after subtracting the day 34 spectrum from the later day 1836 spectrum. The residual represents the extra emission that appears at late times. This residual emission is shown in gray, while the black tracing is a smoothed version of this same residual spectrum. This residual blue emission has a spectral morphology that is very reminiscent of the “blue pseudo continuum” that is often seen in SNe Ibn and SNe IIn that are powered by strong CSM interaction. Figure 10 also shows the late-time (day 905) spectrum of SN 2005ip (red) from Smith et al. (2009b), which was a Type IIn explosion that was unusually bright at late times because of strong and persistent ongoing CSM interaction. With the exception of a few narrow coronal lines that are especially strong in SN 2005ip (Smith et al. 2009b), Figure 10 shows that a late-time SN IIn actually provides quite a good match for the blue excess emission in UGC 2773-OT.

The presence of fast ejecta and a growing contribution to the observed spectra from shock emission is interesting in the context of making comparisons between UGC 2773-OT and the Great Eruption of η Carinae. There are several lines of evidence that point to a strong shock as being im-

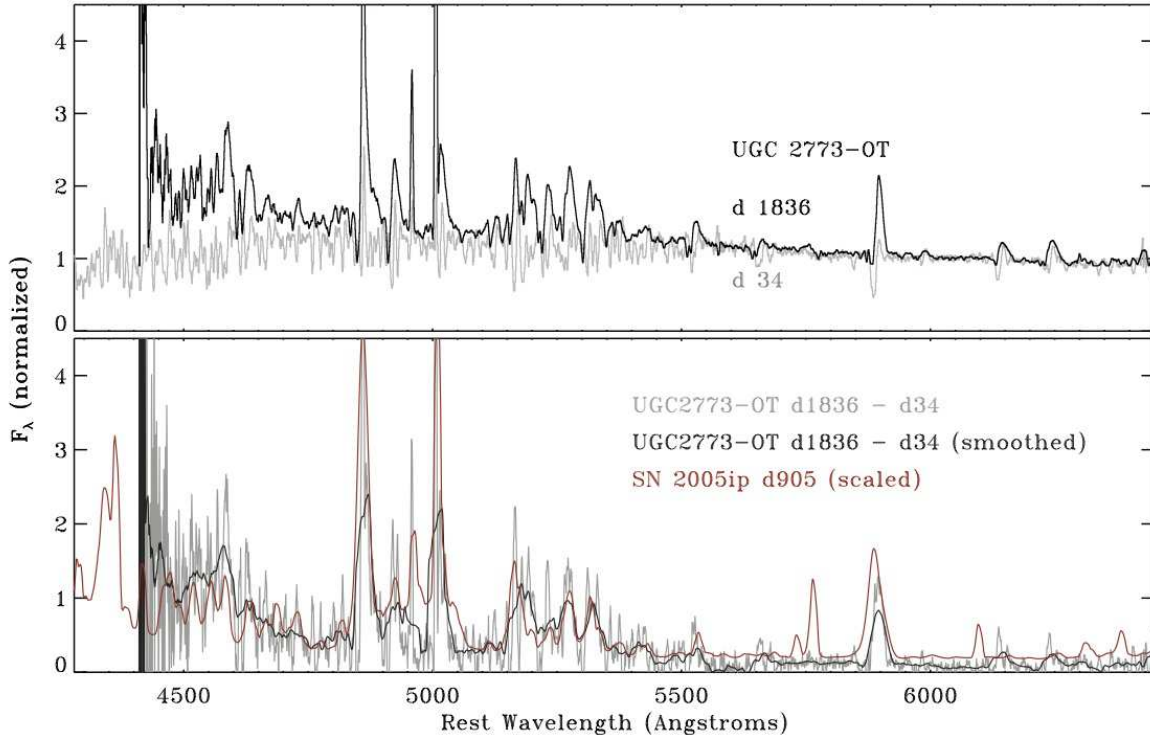


Figure 10. A comparison of the early and late-time spectra for UGC 2773-OT, highlighting the excess blue emission. The top panel shows the day 1836 spectrum (black) compared to the day 34 spectrum from Smith et al. (2010) in gray. Both spectra are normalised to the red continuum level, and in fact the red spectra appear very similar except for $H\alpha$ and Ca^+ . In the blue there is a clear excess of line emission at late times. The bottom panel isolates this excess blue emission by subtracting the normalised day 34 spectrum from the normalised day 1836 spectrum. The gray plot is the residual, and the black plot is a smoothed version of the residual emission. We compare this to the excess “blue pseudo-continuum” seen in SN 2005ip (red) on day 905 (Smith et al. 2009b), which is characteristic of the forest of blue emission lines seen in interacting SNe. This indicates that the excess blue line emission in UGC 2773-OT is most likely powered by a shock interacting with CSM.

portant for powering η Car’s Great Eruption: (1) The very fast ejecta outside the Homunculus, moving at speeds of $3000\text{--}5000\text{ km s}^{-1}$ (Smith 2008), which are hard to achieve in a wind model that can also form the slower Homunculus (Owocki et al. 2004), (2) the large ratio of kinetic energy to total radiated energy that exceeds unity (Smith et al. 2003), (3) the very thin walls of the Homunculus nebula that seem to have been compressed in a radiative shock (Smith 2006), and (4) spectra of light echoes of η Car that seem inconsistent with expectations for an opaque wind model (Rest et al. 2012; Prieto et al. 2014). These indicators of explosive mass loss seem, at first glance, to be at odds with the decade-long duration of the bright plateau in η Car, which is of course much longer than the short duration of hydrodynamic mass ejection. Using a simple 1-D model of CSM interaction, however, Smith (2013) showed that the long plateau of η Car’s 19th century event could be powered by CSM interaction by adopting physical parameters that are consistent with the mass and kinetic energy now observed in the Homunculus. The fact that observed spectra of the UGC2773-OT transient show evidence for an increasing contribution from shock-powered emission reinforces the conclusion that shocks play an important role in powering the long-duration high-luminosity plateaus of these two events, and also bolsters the comparison between UGC2773-OT and η Car (note

that spectra of light echoes corresponding to η Car’s long 1850s plateau are still being analyzed; Smith et al., in prep.).

Some observed evidence for strong shock excitation has been reported for other SN impostors as well, usually showing a characteristically “hot” spectrum (see Smith et al. 2011). Some of these are the pre-SN eruptions of SN 2009ip (Smith et al. 2010; Foley et al. 2011), SN 2000ch (Smith et al. 2011; Pastorello et al. 2010; Wagner et al. 2004), and SNHunt248 (Mauerhan et al. 2015). All of these, however, have exhibited brief luminosity spikes (weeks to months), not sustained decade-long events like η Carinae and UGC 2773-OT.

4.2 Asymmetry in the Ejecta

One of the most remarkable aspects of the spectral evolution of UGC 2773-OT in its first 2000 days is its $H\alpha$ line (Figure 4). In particular, we note the change in profile shape from a normal P Cyg profile that one might attribute to a moderately slow wind, to a multi-peaked and asymmetric pure emission profile, accompanied by a huge increase in strength of $H\alpha$ emission.

As noted above, various spectral clues suggest a significant contribution to the optical emission from shock excited gas in CSM interaction. This is especially true for $H\alpha$, where shock excitation likely dominates the broad ($\pm 1000\text{ km s}^{-1}$)

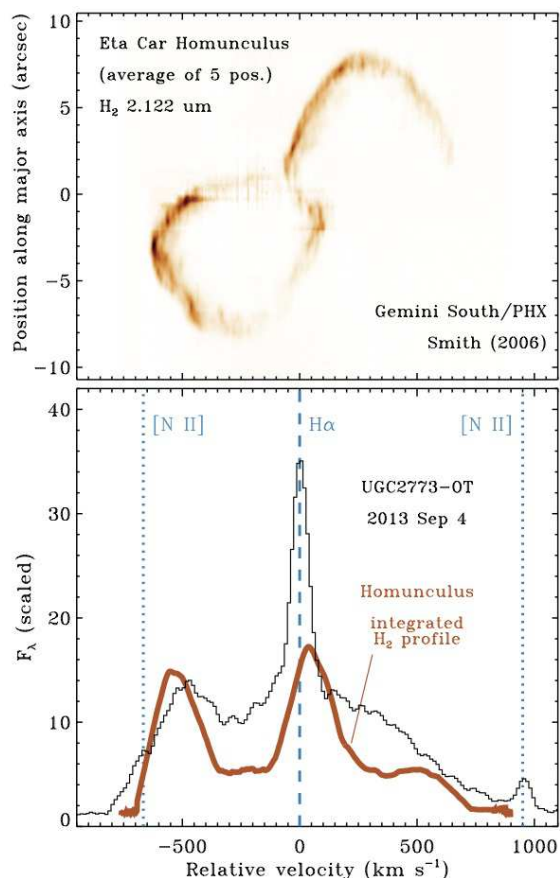


Figure 11. Comparison between the asymmetric $H\alpha$ line profile observed in UGC 2773-OT to the H_2 emission from the Homunculus nebula around η Carinae. The top panel shows the 2D long-slit spectrum of H_2 S(1-0) 2.122 μm emission from the Homunculus. This is an average of 5 adjacent slit positions with the slit aligned along the major (polar) axis of the bipolar nebula, excluding a region around the bright central star. These H_2 spectra were obtained with the Phoenix spectrograph on Gemini South, and the individual positions were presented by Smith (2006). The bottom panel compares the line profile of this H_2 emission integrated along the slit (meant to mimic the integrated H_2 line profile observed for the whole Homunculus nebula). This is the thick orange curve, which is compared to the $H\alpha$ profile observed in UGC 2773-OT (black) on 2013 Sep. 4.

$H\alpha$ luminosity. While the earliest epoch showed a similar line profile in $H\alpha$ and $H\beta$, the late-time $H\beta$ does not show a broad multi-peaked line profile like $H\alpha$, and it does not exhibit a comparable increase in strength. In fact, no other emission line in the spectrum shows a profile similar to that of $H\alpha$. This argues that the strong $H\alpha$ emission is caused by shock excitation in a similar vein to the strong $H\alpha$ emission that often dominates the late-time spectra of SNe IIn (e.g., Smith, Mauerhan, & Prieto 2014). In a steady wind, one expects Balmer transitions and other lines to exhibit similar profile shapes.

If we assume that late-time $H\alpha$ emission traces the postshock gas in CSM interaction, then the unusual profile of $H\alpha$ holds important clues about the geometry of the ejecta and CSM. The line became much stronger with time, but the profile shape also changed dramatically. A blue bump of ex-

cess emission appeared in our second epoch of spectra on day 478/479 (see Figure 4). The blue bump was located at roughly -360 km s^{-1} , which is roughly the same speed as the P Cygni absorption trough in the first epoch on day 34 (Smith et al. 2010). (This blue bump is not at the correct wavelength to be $[\text{N II}] \lambda 6548$; see Figure 4.) The blue bump then grew stronger with time and migrated to faster blueshifted speeds. At later times (days 1000-2000) the blue bump is seen at roughly -600 to -800 km s^{-1} , while a corresponding red bump develops as well (although less pronounced). At later times the $H\alpha$ profile exhibits very steep blue and red wings, unlike the profile wings from electron scattering in a wind.

A qualitatively similar asymmetric blue bump in $H\alpha$ has been seen at different speeds in several SNe IIn (Smith et al. 2012a,b, 2015; Fransson et al. 2014), and is usually attributed bipolar or perhaps disk-like geometry in the shock interaction. A corresponding red bump is usually assumed to be weaker or absent due to extinction by dust or occultation by the opaque SN photosphere. Radiative transfer simulations of SNe IIn with bipolar CSM support these expectations of having an asymmetric blue emission line arising from a bipolar geometry (Dessart et al. 2015). The increasing speed with time seen in UGC 2773-OT is likely due to the dominant emission migrating from the slower preshock CSM to the accelerated post shock gas.

This sign of asymmetry in the line profiles during the eruption has important implications for understanding the origin of bipolar nebulae around LBVs and other massive stars. Since the blue bump is seen from emission lines that arise in CSM interaction during the transient event itself, this requires that the shaping of the bipolar nebula occurs during the event or before (imprinted in the inner CSM), and is not due to hydrodynamic shaping over a long time after the event. So, for example, the bipolar nebula seen centuries or thousands of years later does not arise from an asymmetric posteruption wind, nor from interaction between a wind and an extended disk-like CSM at large radii. The bipolar geometry must be inherent to the physics of the explosion itself, or to the CSM ejected immediately before that is overtaken by the ejecta during the observed event.

In this paper we have compared UGC 2773-OT's recent long-lasting eruption to the historical 19th century eruption of η Carinae (Smith & Frew 2011). In that spirit, Figure 11 makes another relevant comparison. This figure shows the asymmetric $H\alpha$ line profile observed at late times in UGC 2773-OT, and compares it to the present-day line profile of emission from the Homunculus nebula around η Car. At the present epoch, η Car's ejecta have cooled and the nebula is seen as a dusty reflection nebula at visible wavelengths, rather than in $H\alpha$ emission. However, the dense thin shell that contains most of the mass in the Homunculus emits bright near-IR H_2 lines (Smith 2006). In the CSM interaction model proposed by Smith (2013), the thin walls of the Homunculus seen today in H_2 correspond to the cold dense shell of postshock gas that would have emitted bright $H\alpha$ during the eruption. Therefore, the comparison in Figure 11 is physically motivated, because the different lines are tracing essentially the same postshock gas, before or after it cools. The H_2 emission line profile shown here is an attempt to mimic the integrated H_2 profile of the entire nebula, as if the Homunculus were an unresolved point source at a large

distance. This is accomplished by summing the H_2 emission along the slit, for the several different slits used to map the Homunculus with the Phoenix spectrograph at Gemini South. These data were originally presented and discussed by Smith (2006). The result of this exercise is that the integrated H_2 emission from the Homunculus nebula shows a profile that is very similar to that of the $H\alpha$ emission observed now in UGC 2773-OT. A strong blue bump is seen from the front of the approaching blueshifted polar lobe of the nebula, and a central peak is seen from slower material at the pinched waist of the nebula. The emission peak from the receding polar lobe is suppressed in this case by dust extinction in the Homunculus (Smith 2006). This comparison makes a strong plausibility argument that the $H\alpha$ profile seen in UGC 2773-OT could arise in a bipolar shell created by CSM interaction, as in η Car, and it underscores the potential similarity of the two objects.

At late times, lines of [Ca II] and Ca II also exhibit unusual and asymmetric profile shapes (Figure 9), and the emission components trace different velocities than $H\alpha$. The forbidden lines of the [Ca II] $\lambda\lambda 7291, 7324$ are not contaminated by absorption. Their profiles are quite boxy, with double peaked horns at the relatively flat top of the profile, and their steep line wings extend only to about half the velocity seen in $H\alpha$. Such differences are not expected in a wind where radiation scatters out from a central source, and where forbidden lines would presumably trace the outermost material at the final coasting velocity (faster than in the inner wind acceleration region). Instead, the stark differences in line profile shape and width between $H\alpha$ and [Ca II] may arise because they trace different latitudinal zones in the shock front. A bipolar shock front will have significantly different speeds – and hence different excitation/ionization levels – at the slow equator and fast poles. $H\alpha$ may trace the stronger and faster shock at the polar regions of the bipolar shock, whereas [Ca II] emission may be restricted to lower speed and lower excitation material near the equator or mid latitudes. The fact that the IR triplet Ca II lines show these faster speeds in absorption that are similar to $H\alpha$ emission supports this conjecture.

4.3 A Key Difference

Although we have discussed above how UGC 2773-OT bears many observable similarities to the historical 19th century eruption of η Carinae, there is one key difference that needs to be mentioned. This difference stems from the fact that UGC 2773-OT shows a smooth light curve, whereas η Car shows a series of repeating brief luminosity spikes in its historical data (Smith & Frew 2011), especially before 1845, as noted in the Introduction.

These brief luminosity spikes seem to coincide with times of periastron passage in the very eccentric binary system if we extend the present day 5.5 yr orbit back in time, with a small adjustment to the period for the mass lost in the event (Smith & Frew 2011; Damineli 1996). The periastron events have been discussed in terms of grazing stellar collisions at periastron due to an inflated primary star's envelope (Smith 2011), and periastron accretion events onto a companion that power the event and blow jets that shape the bipolar Homunculus (Soker 2001; Kashi & Soker 2009). If these brief encounters are missing in UGC 2773-OT but

it produces a long-lived eruption and a bipolar nebula anyway, we may be receiving a clue that the periastron collisions could be a secondary effect rather than the driving mechanism of these eruptions. This last point is speculative, however, and additional examples of similarly persistent LBV giant eruptions with well-sampled photometry would be valuable in this regard.

ACKNOWLEDGEMENTS

We thank an anonymous referee for a careful reading of the manuscript. We thank the staffs at the MMT, LBT, Bok, Lick, and Keck Observatories for their assistance with the observations. We thank Charles Kilpatrick for assistance with some of the Kuiper observing, and Betsy Green for assistance with Bok observations. Observations using Steward Observatory facilities were obtained as part of the large observing program AZTEC: Arizona Transient Exploration and Characterization. Some observations reported here were obtained at the MMT Observatory, a joint facility of the University of Arizona and the Smithsonian Institution. This research was also based in part on observations made with the LBT. The LBT is an international collaboration among institutions in the United States, Italy and Germany. The LBT Corporation partners are the University of Arizona on behalf of the Arizona university system; the Istituto Nazionale di Astrofisica, Italy; the LBT Beteiligungsgesellschaft, Germany, representing the Max-Planck Society, the Astrophysical Institute Potsdam and Heidelberg University; the Ohio State University and the Research Corporation, on behalf of the University of Notre Dame, University of Minnesota and University of Virginia. Some of the data presented herein were obtained at the W.M. Keck Observatory, which is operated as a scientific partnership among the California Institute of Technology, the University of California, and NASA; the observatory was made possible by the generous financial support of the W.M. Keck Foundation. The authors wish to recognise and acknowledge the very significant cultural role and reverence that the summit of Mauna Kea has always had within the indigenous Hawaiian community. We are most fortunate to have the opportunity to conduct observations from this mountain. Based in part on observations obtained at the Gemini Observatory, which is operated by AURA, under a cooperative agreement with the NSF on behalf of the Gemini partnership: the National Science Foundation (US), the Particle Physics and Astronomy Research Council (UK), the National Research Council (Canada), CONICYT (Chile), the Australian Research Council (Australia), CNPq (Brazil), and CONICET (Argentina). Research at Lick Observatory is partially supported by a generous gift from Google.

N.S.'s research on Eta Carinae and related eruptions receives support from NSF grants AST-1312221 and AST-1515559, as well as from NASA grant AR-12618 from the Space Telescope Science Institute, which is operated by Associated Universities for Research in Astronomy, Inc., under NASA contract NAS 5-26555. The supernova research of A.V.F.'s group at U.C. Berkeley is supported by Gary & Cynthia Bengier, the Richard & Rhoda Goldman Fund, the Christopher R. Redlich Fund, the TABASGO Foundation, and NSF grant AST-1211916. KAIT and its ongoing operation were made possible by donations from Sun Microsystems, Inc., the Hewlett-Packard Company, AutoScope Corporation, Lick Observatory, the NSF, the University of California, the Sylvia & Jim Katzman Foundation, and the TABASGO Foundation.

REFERENCES

- Berger E., et al., 2009, *ApJ*, 699, 1850
- Boles T., 2009, *CBET*, 1931, 1
- Bond H., Bedin L. R., Bonanos A. Z., Humphreys R. M., Monard L. A. G. B., Prieto J. L., Walter F. M., 2009, *ApJ*, 695, L154
- Damineli A. 1996, *ApJ*, 460, L49
- Davidson K. 1987, *ApJ*, 317, 760
- Davidson K. et al., 1986, *ApJ*, 305, 867
- de Koter A., Lamers H.J.G.L.M., Schmutz W. 1996, *A&A*, 306, 501
- Dessart L., Audi E., Hillier D.J. 2015, *MNRAS*, 449, 4304
- Drissen L., Crowther P. A., Smith L. J., Robert C., Roy J. R., Hillier D. J., 2001, *ApJ*, 546, 484
- Faber S.M., et al. 2003, in Tyson J. A., Wolff S., eds, *SPIE Conf. Ser. Vol. 4836, Instrument Design and Performance for Optical/Infrared Ground-based Telescopes*. SPIE, Bellingham, p. 1657
- Filippenko A.V. 1982, *PASP*, 94, 715
- Filippenko A.V. 2003, in *From Twilight to Highlight: The Physics of Supernovae*, ed. W. Hillebrandt & B. Leibundgut (Berlin: Springer), 171
- Foley R.J., Berger E., Fox O., et al. 2011, *ApJ*, 732, 32
- Fransson C., et al. 2014, *ApJ*, 797, 118
- Goodrich R. W., Stringfellow G. S., Penrod G. D., Filippenko A. V., 1989, *ApJ*, 342, 908

- Graefner G., Owocki S.P., Vink J. 2012, *A&A*, 538, A40
- Groh J.H., Hillier D.J., Damineli A., Whitelock P.A., Marang F., Rossi C. 2009a, *ApJ*, 698, 1698
- Groh J.H., et al. 2009b, *ApJ*, 705, L25
- Herschel J.F.W. 1847, *Results of Astronomical Observations Made... at the Cape of Good Hope*. Smith, Elder & Co., London
- Humphreys R.M., Davidson K., 1994, *PASP*, 106, 1025
- Humphreys R.M., Davidson K., 1994, *PASP*, 111, 1124
- Kashi A., Soker N. 2009, *New Astron.*, 14, 11
- Kochanek, C.S. 2011, *ApJ*, 743, 73
- Kochanek, C.S., Szczygiel, D.M., & Stanek, K.Z. 2011, *ApJ*, 737, 76
- Kochanek, C.S., Szczygiel, D.M., & Stanek, K.Z. 2012, *ApJ*, 758, 142
- Kochanek C.S., Adams S.M., Belczynski K. 2014, *MNRAS*, 443, 1319
- Koenigsberger G., 2004, *Rev. Mex. Astron. Astrofis.*, 40, 107
- Li, W., Filippenko, A. V., Van Dyk, S. D., Hu, J., Qiu, Y., Modjaz, M., & Leonard, D. C. 2002, *PASP*, 114, 403
- Mauerhan J.C., Smith N., Filippenko, A.V., et al. 2013, *MNRAS*, 430, 1801
- Mauerhan J.C., et al. 2015, *MNRAS*,
- Maund J.R., et al. 2006, *MNRAS*, 369, 390
- Oke J.B., Cohen J.G., Carr M., et al. 1995, *PASP*, 107, 375
- Owocki S. P., Gayley K. G., Shaviv N. J., 2004, *ApJ*, 616, 525
- Pastorello A., et al. 2010, *MNRAS*, 408, 191
- Podsiadlowski P. 2010, *New Astron. Rev.*, 54, 39
- Prieto J. L. 2008, *ATel*, 1550, 1
- Prieto J. L. et al. 2008a, *ApJ*, 681, L9
- Prieto J. L., Kistler M. D., Stanek K. Z., Thompson T. A., Kochanek C. S., Beacom J. F., 2008b, *The Astronomers Telegram*, 1596, 1
- Prieto J.L., et al. 2014, *ApJ*, 787, 8
- Rest, A., et al. 2012, *Nature*, 482, 375
- Smith N. 2006, *MNRAS*, 644, 1151
- Smith N. 2008, *Nature*, 455, 201
- Smith N. 2011, *MNRAS*, 415, 2020
- Smith N. 2013, *MNRAS*, 429, 2366
- Smith N. 2014, *ARAA*, 52, 487
- Smith N., Morse J. A., 2004, *ApJ*, 605, 854
- Smith N., Frew, D. 2011, *MNRAS*, 415, 2009
- Smith N., Tombleson R. 2015, *MNRAS*, 447, 602
- Smith N., Gehrz R. D., Hinz P. M., Hoffmann W. F., Hora J. L., Mamajek E. E., Meyer M. R., 2003, *AJ*, 125, 1458
- Smith N., et al. 2009a, *MNRAS*, 695, 1334
- Smith N., Ganeshalingam M., Chornock R., et al. 2009b, *ApJ*, 697, L49
- Smith N., Miller A., Li W., et al. 2010, *AJ*, 139, 1451
- Smith N., et al. 2011, *MNRAS*, 415, 773
- Smith N., et al. 2012a, *AJ*, 143, 17
- Smith N., et al. 2012b, *MNRAS*, 420, 1135
- Smith N., Mauerhan J.C., Prieto J.L. 2014, *MNRAS*, 438, 1191
- Smith N., et al. 2015, *MNRAS*, 449, 1876
- Soker N., 2001, *MNRAS*, 325, 584
- Szczygiel DM, Kochanek CS, Dai X. 2012, *ApJ*, 760, 20
- Thompson T. A., Prieto J. L., Stanek K. Z., Kistler M. D., Beacom J. F., Kochanek C. S., 2009, *ApJ*, 705, 1364
- Van Dyk S. D., 2005, in Humphreys R. M., Stanek K. Z., eds, *ASP Conf. Ser. Vol. 332, The Fate of the Most Massive Stars* (Astron. Soc. Pac., San Francisco), p. 47
- Van Dyk S. D., Peng C. Y., King J. Y., Filippenko A. V., Treffers R. R., Li W., Richmond M. W., 2000, *PASP*, 112, 1532
- Van Dyk S. D., Li W., Filippenko A. V., Humphreys R.M., Foley R., Challis P., 2006, preprint (astro-ph/0603025)
- Van Dyk S.D., Matheson T. 2012, in *Eta Carinae and the Supernova Impostors*, ed. R.M. Humphreys and K. Davidson (Springer)
- Wagner R.M., et al., 2004, *PASP*, 116, 326
- Wesson, R., et al. 2010, *MNRAS*, 403, 474
- Zwicky, F. 1961, *ApJ*, 139, 514
- Zwicky, F. 1965, in *Stars and Stellar Systems*, ed. L.H. Aller & D.B. McLaughlin (Chicago: U. Chicago Press)